Inorganic Chemistry

Article

Tuning the Electronic Structure of Octahedral Iron Complexes [FeL(X)] (L = 1-Alkyl-4,7-bis(4-*tert*-butyl-2-mercaptobenzyl)-1,4,7-triazacyclononane, X = Cl, CH₃O, CN, NO). The $S = {}^1/_2 \rightleftharpoons S = {}^3/_2$ Spin Equilibrium of [FeL^{Pr}(NO)]

Ming Li,[†] **Didier Bonnet,**[†] **Eckhard Bill,**[†] **Frank Neese,**[†] **Thomas Weyhermüller,**[†] **Nicole Blum,**[‡] **Dieter Sellmann,**[‡] **and Karl Wieghardt*,**[†]

Max-Planck-Institut für Strahlenchemie, Stiftstrasse 34-36, D-45470 Mülheim an der Ruhr, Germany, and Institut für Anorganische Chemie der Universität Erlangen-Nürnberg, Egerlandstrasse 1, D-91058 Erlangen, Germany

Two new pentadentate, pendent arm macrocyclic ligands of the type 1-alkyl-4,7-bis(4-*tert*-butyl-2-mercaptobenzyl)-1,4,7-triazacyclononane where alkyl represents an isopropyl, (L^{Pr})$^{2-}$, or an ethyl group, (L^{Et})$^{2-}$, have been synthesized. It is shown that they bind strongly to ferric ions generating six-coordinate species of the type [Fe(L^{alk})X]. The ground state of these complexes is governed by the nature of the sixth ligand, X: [Fe^{III}(L^{Et})Cl] (**2**) possesses an $S = {}^5/_2$ ground state as do [Fe^{III}(L^{Et})(OCH₃)] (**3**) and [Fe^{III}(L^{Pr})(OCH₃)] (**4**). In contrast, the cyano complexes [Fe^{III}-(L^{Et})(CN)] (**5**) and [Fe^{III}(L^{Pr})(CN)] (**6**) are low spin ferric species ($S = {}^1/_2$). The octahedral {FeNO}^{7} nitrosyl complex [Fe(L^{Pr})(NO)] (**7**) displays spin equilibrium behavior $S = {}^1/_2 \rightleftharpoons S = {}^3/_2$ in the solid state. Complexes [Zn(L^{Pr})] (**1**), **4**·CH₃OH, **5**·0.5toluene·CH₂Cl₂, and **7**·2.5CH₂Cl₂ have been structurally characterized by low-temperature (100 K) X-ray crystallography. All iron complexes have been carefully studied by zero- and applied-field Mössbauer spectroscopy. In addition, Sellmann's complexes [Fe(pyS₄)(NO)]$^{0/1+}$ and [Fe(pyS₄)X] (X = PR₃, CO, SR₂) have been studied by EPR and Mössbauer spectroscopies and DFT calculations (pyS₄ = 2,6-bis(2-mercaptophenylthio-methyl)pyridine(2–)). It is concluded that the electronic structure of **7** with an $S = {}^1/_2$ ground state is low spin ferrous ($S_{Fe} = 0$) with a coordinated neutral NO radical (Fe^{II}–NO) whereas the $S = {}^3/_2$ state corresponds to a high spin ferric ($S_{Fe} = {}^5/_2$) antiferromagnetically coupled to an NO$^-$ anion ($S = 1$). The $S = {}^1/_2 \rightleftharpoons S = {}^3/_2$ equilibrium is then that of valence tautomers rather than that of a simple high spin $\rightleftharpoons$ low spin crossover.

Introduction

Six-coordinate (nitrosyl)iron complexes containing an {Fe–NO}^{7} core according to the Enemark and Feltham nomenclature[1] have been shown to possess an $S = {}^3/_2$ [2–6] or ${}^1/_2$ [7–9] ground state. Non-heme ferrous centers in a number of metalloproteins react reversibly with NO with formation of paramagnetic nitrosyl species ($S = {}^3/_2$).[2,9–15] We[6] and others[16,17] have shown by X-ray absorption, resonance

* To whom correspondence should be addressed. E-mail: wieghardt@mpi-muelheim.mpg.de.
† Max-Planck-Institut für Strahlenchemie.
‡ Institut für Anorganische Chemie der Universität Erlangen-Nürnberg.

(1) Enemark, J. H.; Feltham, R. D. *Coord. Chem. Res.* **1974**, *13*, 339.
(2) Arciero, D. M.; Lipscomb, J. D.; Huynh, B. H.; Kent, T. A.; Münck, E. *J. Biol. Chem.* **1983**, *258*, 14981.
(3) Wells, F. V.; McCann, S. W.; Wickman, H. H.; Kessel, S. L.; Hendrickson, D. N.; Feltham, R. D. *Inorg. Chem.* **1982**, *21*, 2306.
(4) Teig, A.; Bautista, M. T.; Lippard, S. J. *Inorg. Chem.* **1996**, *35*, 6892.
(5) Pohl, K.; Wieghardt, K.; Nuber, B.; Weiss, J. *J. Chem. Soc., Dalton Trans.* **1987**, 187.
(6) Hauser, C.; Glaser, T.; Bill, E.; Weyhermüller, T.; Wieghardt, K. *J. Am. Chem. Soc.* **2000**, *122*, 4352.
(7) Sellmann, D.; Blum, N.; Heinemann, F. W.; Hess, B. A. *Chem. Eur. J.* **2000**, *7*, 1874.
(8) Enemark, J. H.; Feltham, R. D.; Huie, B. T.; Johnson, P. L.; Bizot Swedo, K. *J. Am. Chem. Soc.* **1977**, *99*, 3285.
(9) Nasri, H.; Ellison, M. K.; Chen, S.; Huynh, B. H.; Scheidt, W. R. *J. Am. Chem. Soc.* **1997**, *119*, 6274.
(10) Nocek, J. M.; Kurtz, D. M., Jr.; Sage, J. T.; Xia, Y.-M.; Debrunner, P.; Shiemke, A. K.; Sanders-Loehr, T. M. *Biochemistry* **1988**, *27*, 1014.
(11) Rodriguez, J. H.; Xia, Y.-M.; Debrunner, P. *J. Am. Chem. Soc.* **1999**, *121*, 7846.
(12) Bill, E.; Berhardt, F.-H.; Trautwein, A. X.; Winkler, H. *Eur. J. Biochem.* **1985**, *147*, 177.
(13) Haskin, C. J.; Ravi, N.; Lynch, J. B.; Münck, E.; Que, L., Jr. *Biochemistry* **1995**, *34*, 11090.
(14) Chen, V. J.; Orville, A. M.; Harpel, M. R.; Frolik, C. A.; Sureros, K.; Münck, E.; Lipscomb, J. D. *J. Biol. Chem.* **1989**, *264*, 21677.

Chart 1. [Fe(NO)(pyS₄)]$^{0/1+}$ Complexes

Scheme 1. Ligands and Complexes
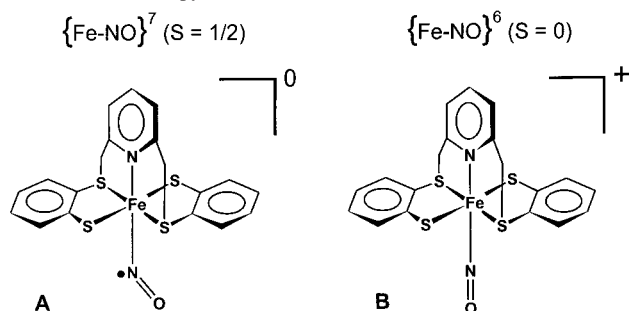
Raman, magnetic circular dichroism, electron paramagnetic resonance, Mössbauer spectroscopies, and, in addition, SCF-Xα-SW and GGA density functional calculations that these $\{Fe-NO\}^7$ ($S = \frac{3}{2}$) species are high spin ferric ($S = \frac{5}{2}$) antiferromagnetically coupled to NO^- ($S = 1$).

Recently, Sellmann et al.[7] have reported the two structurally characterized (nitrosyl)iron species **A** and **B**, where the latter is a diamagnetic $\{Fe-NO\}^6$ ($S = 0$) and the former is a paramagnetic $\{Fe-NO\}^7$ ($S = \frac{1}{2}$) species (Chart 1).
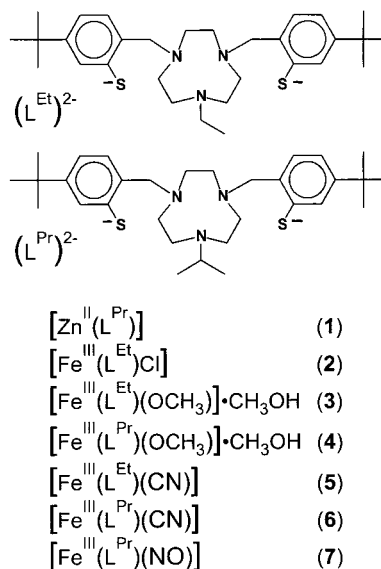
Here, we report a new six-coordinate $\{Fe-NO\}^7$ species, and we will attempt to describe its electronic structure. It represents the first spin equilibrium example $S = \frac{1}{2} \rightleftharpoons S = \frac{3}{2}$ of a six-coordinate (nitrosyl)iron complex of type $\{Fe-NO\}^7$. Some examples of five-coordinate species have been reported previously.[3,18−20] The pentadentate macrocyclic pendent arm ligands 1-isopropyl-4,7-(4-*tert*-butyl-2-mercaptobenzyl)-1,4,7-triazacyclononane, $(L^{Pr})^{2-}$, and its 1-ethyl derivative, $(L^{Et})^{2-}$, described here, bind strongly to ferric ions (Scheme 1). The vacant sixth coordination site can then be occupied by chloride, methoxide, cyanide, and nitrosyl ligands. The nature of this sixth ligand determines the electron configuration at the iron ion. Thus, the chloro and methoxo complexes are high spin ferric whereas the cyanide complexes are low spin configurated. As indicated previously, the nitrosyl complex [Fe(L^{Pr})(NO)] exhibits a temperature dependent $S = \frac{1}{2} \rightleftharpoons S = \frac{3}{2}$ spin equilibrium in the solid state.

The present work was also undertaken to demonstrate the strength of zero- and applied-field Mössbauer spectroscopy in combination with DFT in elucidating the correct electronic structure of non-heme (nitrosyl)iron complexes.

Experimental Section

Preparation of the Ligands H₂L^{Pr} and H₂L^{Et}. All air-sensitive manipulations were carried out by standard Schlenk line techniques. 4-*tert*-Butyl-2-nitrobenzaldehyde and [1,4,7]triazonane-1,4-dicar-

boxylic acid di-*tert*-butyl ester were prepared according to published procedures.[21,22,41]

2-(4-Methoxybenzylsulfanyl)-4-*tert*-butyl-benzaldehyde (a). To a solution of 4-*tert*-2-nitrobenzaldehyde (70 g; 0.34 mol) in degassed DMF (90 mL) was added K₂CO₃ (73 g, 0.53 mol) and 4-methoxybenzal mercaptan (47 mL), subsequently. The reaction mixture was stirred under Ar at 80 °C for 12 h. After cooling, the solution was added to water (1 L) at 0 °C and extracted with diethyl ether which was washed with water two times. The ether phase was dried over Na₂SO₄, and the solvent was removed by rotary evaporation. A brown-red oil dissolved in methanol was stored for a couple of days at −10 °C. A solid was obtained, which was filtered off and washed with *n*-hexane. Yield: 50.2 g. ¹H NMR (CDCl₃, 500 MHz): δ 10.28 (s, 1H), 7.74 (d, $J = 8.13$ Hz, 1H), 7.35 (d, $J = 1.73$ Hz, 1H), 7.31 (dd, $J = 8.13$ Hz, $J = 1.73$ Hz, 1H), 7.14 (d, $J = 6.65$ Hz, 2H), 6.78 (d, $J = 6.65$ Hz, 2H), 4.06 (s, 2H), 3.75 (s, 3H), 1.25 (s, 9H). ¹³C{¹H}NMR (CDCl₃, 125 MHz): δ 191.37, 158.98, 157.75, 132.79, 130.93, 129.99, 128.50, 128.25, 123.83, 114.03, 55.56, 38.88, 35.37, 30.91 ppm. EIMS: $m/z = 121(100)$, 314(M⁺).

[2-(4-Methoxybenzylsulfanyl)-4-*tert*-butylphenyl]-methanol (b). To a solution of aldehyde **a** (26.6 g; 0.085 mol) in ethanol (40 mL) was added NaBH₄ (3.5 g, 0.09 mol) in small amounts with stirring at 0 °C. After removal of the solvent ethanol, the residue was dissolved in diethyl ether, washed with H₂O, dried over Na₂SO₄, and filtered. The solvent was removed by evaporation under reduced pressure to afford a brown oil (24.4 g). ¹H NMR (CD₂Cl₂, 250 MHz): δ 7.33 (s, 1H), 7.27 (q, 2H), 7.12 (d, $J = 8.55$ Hz, 2H), 6.78 (d, $J = 8.85$ Hz, 2H), 4.63 (d, $J = 6.25$ Hz, 2H), 4.03 (s, 2H), 3.75 (s, 3H), 2.02 (t, $J = 6.25$ Hz, 1H), 1.26 (s, 9H). ¹³C{¹H} NMR (CD₂Cl₂, 62 MHz): δ 159.26, 151.62, 139.62, 133.77, 130.32, 130.01, 128.47, 124.78, 114.16, 63.65, 55.57, 39.60, 34.86, 31.32 ppm. EIMS: $m/z = 121(100)$, 316(M⁺).

1-Bromomethyl-2-(4-methoxybenzylsulfanyl)-4-*tert*-butyl-phenyl (c). A solution of PBr₃ (10 g; 0.03 mol) in CHCl₃ (100 mL) was added dropwise to a solution of alcohol **b** (24.4 g; 0.08 mol) in CHCl₃ (120 mL) at 0 °C and stirred for 30 min. Water

(15) Orville, A. M.; Chen, V. J.; Kriauciunas, A.; Harpel, M. R.; Fox, B. G.; Münck, E.; Lipscomb, J. D. *Biochemistry* **1992**, *31*, 4602.

(16) Brown, C. A.; Parlosky, M. A.; Westre, T. E.; Zhang, Y.; Hedman, B.; Hodgson, K. O.; Solomon, E. I. *J. Am. Chem. Soc.* **1995**, *117*, 715.

(17) Westre, T. E.; Di Cicco, A.; Filipponi, A.; Natoli, C. R.; Hedman, B.; Solomon, E. I.; Hodgson, K. O. *J. Am. Chem. Soc.* **1994**, *116*, 6757.

(18) Hodges, K. D.; Wollmann, R. G.; Kessel, S. L.; Hendrickson, D. N.; van Derveer, D. G.; Barefield, E. K. *J. Am. Chem. Soc.* **1979**, *101*, 906.

(19) Haller, K. J.; Johnson, P. L.; Feltham, R. D.; Enemark, J. H.; Ferraro, J. R.; Basile, L. J. *Inorg. Chim. Acta* **1979**, *33*, 19.

(20) Leeuwenkamp, O. R.; Plug, C. M.; Bult, A. *Polyhedron* **1987**, *6*, 295.

(21) Kimura, S.; Bill, E.; Bothe E.; Weyhermüller, T.; Wieghardt, K. *J. Am. Chem. Soc.* **2001**, *123*, 6025.

(22) Itoh, M.; Hagiwara, D.; Kamiza, T. *Tetrahedron Lett.* **1975**, *16*, 4393. (b) Kovacs, Z.; Sherry, A. D. *Tetrahedron Lett.* **1995**, *36*, 9269.

(200 mL) was added. The organic phase was washed repeatedly with water until the aqueous phase is neutral. The organic phase was dried over Na_2SO_4. A brown oil was obtained after evaporation of ether. Yield: 28 g. ^1H NMR ($CDCl_3$, 500 MHz): δ 7.31 (d, J = 8.04 Hz, 1H), 7.25 (d, J = 1.73 Hz, 1H), 7.22 (dd, J = 8.04 Hz, J = 1.73 Hz, 1H), 7.13 (d, J = 8.50 Hz, 2H), 6.78 (d, J = 8.50 Hz, 2H), 4.66 (s, 2H), 4.07 (s, 2H), 3.76 (s, 3H), 1.22 (s, 9H). $^{13}C\{^1H\}$ NMR ($CDCl_3$, 125 MHz): δ 158.82, 152.23, 136.25, 134.88, 130.60, 130.44, 130.35, 129.48, 113.89, 55.32, 55.26, 39.36, 34.69, 31.18 ppm.

1-Isopropyl-4,7-*tert*-butoxycarbonyl-1,4,7-triazacyclononane (d). 1,4-Di(*tert*-butoxycarbonyl)-1,4,7-triazacyclononane (38 g; 0.12 mol), isopropyl bromide (31.3 g; 0.25 mol), Na_2CO_3 (28 g), and tetra-*n*-butylammonium bromide (85 mg) were combined in CH_3-CN (230 mL). The mixture was heated at reflux under argon for 2 days. The yellow mixture was filtered, and the solid was washed with CH_3CN. The combined filtrates were evaporated under reduced pressure to yield a yellow oil (37.7 g, 88%). ^1H NMR ($CDCl_3$, 250 MHz): δ 3.46−3.40 (m, 4H), 3.19−3.14 (m, 4H), 2.83 (septet, J = 6.40 Hz, 1H), 1.43 (s, 18H), 0.92 (d, J = 6.40 Hz, 6H). EIMS: m/z 57(100), 371 (M^+). The corresponding 1-ethyl derivative was prepared analogously using ethylbromide as starting material.

1-Isopropyl-1,4,7-triazacyclononane (e). Concentrated HCl (70 mL) was slowly added to 1-isopropyl-4,7-*tert*-butoxycarbonyl-1,4,7-triazacyclononane (38 g; 0.10 mol). The mixture refluxed for 1 h. After cooling, the resultant solution was adjusted to pH > 10 with aqueous NaOH. The mixture was extracted with $CHCl_3$ (3 × 100 mL). The $CHCl_3$ solution of the product was dried (Na_2SO_4) and the solvent removed under reduced pressure to yield a yellow oil (11 g, 63%). ^1H NMR ($CDCl_3$, 250 MHz): δ 2.76 (septet, J = 6.62 Hz, 1H), 2.67 (s, 4H), 2.64−2.59 (m, 4H), 2.48−2.43 (m, 4H), 0.93 (d, J = 6.62 Hz, 6H). EIMS: m/z 121(100), 767 (M^+). The corresponding 1-ethyl derivative was prepared analogously.

1-Isopropyl-4,7-bis[2-(4-methoxybenzylsulfanyl)benzyl]-1,4,7-triazacyclononane (f). To a solution of 1-isopropyl-1,4,7-triaza-cyclononane (4 g; 23 mmol) in toluene (100 mL) was slowly added a solution of 2-(methoxybenzylthio)-4-*tert*-butylbenzylbromide (22 g; 58 mmol) in toluene (100 mL). After addition of finely powered KOH (5 g), the mixture was heated at 80 °C with stirring overnight. After cooling and filtration, the solvent was removed under reduced pressure to yield an orange-yellow oil. EIMS: m/z 86(100), 171 (M^+). The corresponding 1-ethyl derivative was prepared analogously.

1-Isopropyl-4,7-bis(4-*tert*-butyl-2-mercaptobenzyl)-1,4,7-triazacyclononane Trihydrochloride (H_2L·3HCl) (g). Unpurified 1-isopropyl-4,7-bis[2-(4-methoxybenzylsulfanyl)benzyl]-1,4,7-tri-azacyclononane (29 g) dissolved in degassed tetrahydrofuran (70 mL) was added dropwise to liquid ammonia (∼200 mL) under Ar with stirring. To the mixture was added Na (4.7 g) in small species with vigorous stirring. After the sodium was dissolved, solid NH_4-Cl was added to remove excess sodium. The ammonia was allowed to slowly evaporate by gently heating the solution to room temperature. Degassed aqueous HCl (1 M, 200 mL) was then added to the resultant solution with stirring under argon, the combined solution was extracted with CH_2Cl_2 (3 × 100 mL), the CH_2Cl_2 solution was dried over Na_2SO_4, and the solvent was removed to yield yellow solid (H_2L^{Pr}·3HCl) which was directly used to prepared complexes. ESI (pos. ion): m/z 528 (M^+ + H, 100). The corresponding 1-ethyl derivative, H_2L^{Et}·3HCl, was prepared analogously.

Preparation of Complexes. All preparations were carried out under an argon blanketing atmosphere in order to prevent disulfide formation of the ligands.

[$L^{Pr}Zn$] (1). To a solution of the trishydrochloride of the ligand H_2L^{Pr} (0.64 g; 1.0 mmol) in methanol (20 mL) was added Zn-$(ClO_4)_2$·$6H_2O$ (0.37 g; 1.0 mmol) and 5 equiv of [N(*n*-Bu)$_4$]OH. After stirring for 2 h at 20 °C, a colorless to light yellow precipitate formed which was collected by filtration. Yield: 0.38 g (65%). Single crystals of **1**·1.5 CH_2Cl_2 suitable for X-ray crystallography were grown from CH_2Cl_2 solution. Anal. Calcd for $C_{31}H_{47}N_3S_2Zn$: C, 67.58; H, 8.60; N, 7.63. Found: C, 67.3; H, 8.5; N, 7.4.

[$L^{Et}FeCl$] (2). To a solution of the sodium salt of the ligand, Na_2L^{Et} (0.30 g; 0.54 mmol), in methanol (20 mL) was added $FeCl_3$ (0.043 g; 0.5 mmol). After heating to reflux for 3 h, the solution was cooled to 5 °C for a few hours, after which time a bluish-green powder was collected by filtration and recrystallized from CH_2Cl_2 by slow addition of *n*-pentane. Yield: 25 mg. Anal. Calcd for $C_{30}H_{45}N_3S_2ClFe$: C, 59.75; H, 7.52; N, 6.97. Found: C, 59.6; H, 7.4; N, 7.0. EIMS: m/z = 567 {M − Cl}$^+$. UV−vis (CH_2Cl_2): λ_{max} = 767 (ϵ = 3.8 × 10^3 L mol^{-1} cm^{-1}), 675 (3.4 × 10^3), 471 (2.0 × 10^3), 326 (9.2 × 10^3), 266 (1.5 × 10^4). μ_{eff} (150 K): 5.9 μ_B.

[$L^{Et}Fe(OCH_3)$]CH_3OH (3) and [$L^{Pr}Fe(OCH_3)$]·CH_3OH (4). To a solution of H_2L·3HCl (1.12 g; 1.76 mmol) in methanol (50 mL) were added small pieces of sodium (0.4 g; 17 mmol) with stirring. To the filtered solution was added a solution of [Fe(acac)$_3$] (0.63 g; 1.8 mmol) in CH_3OH (10 mL). The mixture was heated to reflux for 2 h and cooled to −5 °C whereupon blue microcrystals of **4** precipitated. Compound **3** was prepared similarly, but Na_2L^{Pr} was used, and 3 equiv of [N(*n*-Bu)$_4$]OH was added instead of sodium. In both cases, ∼0.4 g of a blue, crystalline material was obtained. Anal. Calcd for $C_{32}H_{52}N_3O_2S_2Fe$ (**3**) and ($C_{33}H_{54}N_3O_2S_2$-Fe (**4**)): C, 60.93 (61.47); H, 8.31 (8.44); N, 6.66 (6.52). Found: C, 60.6 (61.9); H, 8.0 (8.4); N, 7.0 (6.6). EIMS of **3**: m/z = 567 {M − OCH_3}$^+$. **4**: m/z = 581 {M − OCH_3}$^+$. UV−vis (CH_2Cl_2) for **3**: λ = 265 nm (ϵ = 2.2 × 10^4), 608 (2.7 × 10^3). **4**: 230 (2.8 × 10^4), 269 (2.2 × 10^4), 615 (3.4 × 10^3). μ_{eff} for **3**: 5.8 μ_B at 50 K; 6.2 μ_B at 300 K.

[$L^{Et}Fe(CN)$] (5). To a cooled (0 °C) solution of the ligand, Na_2L^{Et}, (0.50 g; 0.9 mmol) in methanol (30 mL) was added [Fe-(acac)$_3$] (0.31 g; 0.9 mmol) whereupon the color of the solution changed to red-brown. After stirring this solution for 10 min at 0 °C, solid NaCN (0.15 g; 3.0 mmol) was added. The solution was gently warmed up to 50 °C and stirred for 20 min during which time a green precipitate formed which was collected by filtration and washed with diethyl ether. Yield: 80−110 mg (15−20%). This material was redissolved in CH_2Cl_2. To the resulting, filtered green solution was added an equal amount of *n*-pentane which initiated the precipitation of a green powder (product C). Alternatively, the volume of the solution was reduced to one-half by evaporation of the solvent CH_2Cl_2 and stored at −40 °C whereupon flat green platelets were obtained within 12 h (product B). When the recrystallization of **C** was slowly performed in a 1:1 mixture of CH_2Cl_2 and *n*-hexane at 20 °C, dark green needles (product A) were obtained within 72 h. Products A, B, and C dried in vacuo for 12 h have been analyzed by elemental analysis. The C, H, and N values are identical within experimental error. Anal. Calcd for $C_{31}H_{45}N_4S_2Fe$: C, 62.72; H, 7.64; N, 9.44. Found: C, 62.5; H, 7.7; N, 9.3. UV−vis (CH_2Cl_2): λ = 265 nm (ϵ = 2.1 × 10^4), 323 (1.4 × 10^4), 467 (850), 664 (2.5 × 10^3), 750 (2.7 × 10^3). μ_{eff} (300 K): 2.1 μ_B. Single crystals suitable for X-ray crystallography of [$L^{Et}Fe(CN)$]0.5 toluene·CH_2Cl_2 were grown from a 1:1 mixture of toluene/CH_2Cl_2. ESIMS: m/z = 593 {M}$^+$.

[$L^{Pr}Fe(CN)$] (6). A solution of H_2L^{Pr}·3HCl (0.64 g; 1.0 mmol), [Fe(acac)$_3$] (0.34 g; 1.0 mol), and [NEt$_4$]CN (0.08 g; 0.5 mmol) in methanol (40 mL), to which triethylamine (2 mL) had been added,

Table 1. Crystallographic Data for **1**·1.5CH$_2$Cl$_2$, **4**·CH$_3$OH, **5**·0.5C$_6$H$_5$CH$_3$·CH$_2$Cl$_2$, and **7**·2.5CH$_2$Cl$_2$

	1·1.5CH$_2$Cl$_2$	**4**·CH$_3$OH	**5**·0.5C$_6$H$_5$CH$_3$·CH$_2$Cl$_2$	**7**·2.5CH$_2$Cl$_2$
formula	C$_{32.5}$H$_{50}$Cl$_3$N$_3$S$_2$Zn	C$_{33}$H$_{54}$FeN$_3$O$_2$S$_2$	C$_{35.5}$H$_{51}$Cl$_2$FeN$_4$S$_2$	C$_{33.5}$H$_{52}$Cl$_5$FeN$_4$OS$_2$
fw	718.60	644.76	724.67	824.01
space group	P$\bar{1}$, No. 2	P2$_1$/n, No. 14	Cmc2$_1$, No. 36	P2$_1$/c, No. 14
a, Å	7.6423(6)	10.0667(8)	23.565(5)	15.3331(8)
b, Å	13.4672(10)	14.4530(12)	14.253(3)	17.6575(8)
c, Å	18.6234(14)	23.078(2)	22.849(5)	14.9283(8)
α, deg	93.15(2)	90	90	90
β, deg	94.11(2)	93.69(2)	90	101.72(2)
γ, deg	106.29(2)	90	90	90
V, Å	1829.4(2)	3350.7(5)	7674(3)	3957.5(3)
Z	2	4	8	4
T, K	100(2)	100(2)	100(2)	100(2)
ρ calcd, g cm^{-3}	1.305	1.278	1.254	1.383
diffractometer	Nonius Kappa-CCD	Nonius Kappa-CCD	Siemens SMART	Nonius Kappa-CCD
reflns collected/θ$_{max}$	19815/31.00	23552/27.50	13710/22.49	39539/30.00
unique reflns/$I > 2\sigma(I)$	11563/8933	7617/5219	4301/3252	11486/7802
no. params/restraints	374/32	389/0	390/3	424/0
μ(Mo Kα), cm^{-1}	10.30	6.08	6.70	8.56
R1^a/GOF^b	0.0645/1.016	0.0517/1.018	0.0864/1.034	0.0580/1.025
wR2^c ($I > 2\sigma(I)$)	0.1595	0.0973	0.2164	0.1384

^{a} Observation criterion: $I > 2\sigma(I)$. R1 $= \sum||F_o| - |F_c||/\sum|F_o|$. ^{b} GOF $= [\sum[w(F_o^2 - F_c^2)^2]/(n - p)]^{1/2}$. ^{c} wR2 $= [\sum[w(F_o^2 - F_c^2)^2]/\sum[w(F_o^2)^2]]^{1/2}$ where $w = 1/\sigma^2(F_o^2)+(aP)^2+bP$, $P = (F_o^2 + 2F_c^2)/3$.

was heated to reflux for 1 h. The filtered solution was cooled to 10 °C whereupon a black-green, microcrystalline material precipitated. Yield: 0.3 g (50%). Anal. Calcd for C$_{32}$H$_{47}$N$_4$S$_2$Fe: C, 63.25; H, 7.80; N, 9.22. Found: C, 63.1; H, 7.8; N, 9.0. EIMS: $m/z = 581$ {M − CN}$^+$, 606 {M − H}$^+$. UV−vis (CH$_2$Cl$_2$): $\lambda = 232$ ($\epsilon = 1.8 \times 10^4$ L mol^{-1} cm^{-1}), 265 (2.1 × 10^4), 319 (1.5 × 10^4), 673 (3.0 × 10^3), 752 (2.4 × 10^3).

[L^{Pr}Fe(NO)]·2.5CH$_2$Cl$_2$ (7). Through a solution of **4** (0.10 g; 0.16 mmol) in degassed CH$_2$Cl$_2$ (20 mL) was passed a stream of purified NO at 20 °C whereupon a color change from blue to purple-red was observed. Slow liquid diffusion of *n*-hexane into the purple-red reaction mixture yielded red-black crystals of [L^{Pr}Fe(NO)]· 2.5CH$_2$Cl$_2$ suitable for X-ray crystallography. Yield: 20 mg (20%). Anal. Calcd for C$_{33.5}$H$_{52}$Cl$_5$N$_4$OS$_2$Fe: C, 48.83; H, 6.36; N, 6.80. Found: C, 48.3; H, 6.1; N, 7.0. EIMS: $m/z = 581$ {M − NO}$^+$. UV−vis (CH$_2$Cl$_2$, 298 K): $\lambda = 232$ nm ($\epsilon = 3.5 \times 10^4$ L mol^{-1} cm^{-1}), 271 (2.0 × 10^4), 289sh (1.9 × 10^4), 539 (2.5 × 10^3).

X-ray Crystallographic Data Collection and Refinement of the Structures. A colorless single crystal of **1**, a dark blue and a green crystal of **4** and **5**, respectively, and a deep red specimen of **7** were coated with perfluoropolyether. Suitable crystals were picked up with a glass fiber and were immediately mounted in the nitrogen cold stream of the diffractometers to prevent loss of solvent. Intensity data were collected at 100 K using graphite monochromated Mo Kα radiation ($\lambda = 0.71073$ Å). Final cell constants were obtained from a least-squares fit of a subset of several thousand strong reflections. Data collection was performed by hemisphere runs taking frames at 0.3° (Siemens SMART) and 1.0° (Nonius Kappa-CCD) in ω. Crystal faces of **1** were determined, and the Gaussian absorption correction routine of XPREP^{23} was used to account for absorption effects. A semiempirical absorption correction using the program SADABS^{24} was performed on the data set of **5**. Intensity data of **4** and **7** were not corrected. Crystallographic data of the compounds and diffractometers used are listed in Table 1. The Siemens ShelXTL^{23} software package was used for solution, refinement, and artwork of the structures. The structures were readily solved by direct methods and difference Fourier techniques.

All non-hydrogen atoms except some atoms in disordered parts were refined anisotropically, and hydrogen atoms were placed at calculated positions and refined as riding atoms with isotropic displacement parameters. Problems occurred during the refinement of solvent molecules and *tert*-butyl groups in **1** and **5**. One CH$_2$Cl$_2$ molecule in **1** is well defined, but a second molecule appeared to be severely disordered (around an inversion center). Two sets of Cl positions with restrained Cl···Cl distances were refined with occupation factors of 0.35 and 0.15. The position of the carbon atom could not be determined. A split atom model was used for the refinement of the *tert*-butyl group C(35)−C(38)/C(35X)− C(38X) in **5** each with half occupation. The C−C distances were restrained to be equal. A toluene molecule lying on a crystallographic mirror plane and a CH$_2$Cl$_2$ molecule in **5** were also disordered. Three split positions were used for dichloromethane, and all atoms of the solvent molecules were refined isotropically. The *tert*-butyl group C(26)−C(28) was split on two positions with occupation factors of 0.5 each.

DFT Calculations. The structures of the five complexes [Fe(pyS$_4$)(X)]$^{0/1+}$ with X = NO, CO, PH$_3$, and S(CH$_3$)$_2$ were fully optimized without symmetry constraints. For the NO species, both the neutral {FeNO}^{7} and the cationic {FeNO}^{6} complex were calculated. The TurboMole package^{25} was used in the geometry optimizations. The Becke^{26}−Perdew^{27} gradient corrected density functional was used, and the Coulomb term was approximated with the resolution of the identity (RI) method.^{28} The split-valence plus polarization (SV(P)) basis set of Schäfer et al.^{29}

(23) *ShelXTL V.5*; Siemens Analytical X-ray Instruments, Inc.: Karlsruhe, Germany, 1994.

(24) Sheldrick, G. M. *SADABS*; Universität Göttingen: Göttingen, Germany, 1994.

(25) Ahlrichs, R.; Bär, M.; Baron, H. P.; Bauernschmitt, R.; Böcker, S.; Ehring, M.; Eichkorn, K.; Elliott, S.; Furche, F.; Haase, F.; Häser, M.; Horn, H.; Huber, C.; Huniar, U.; Kattanek, M.; Kölmel, C.; Kollwitz, M.; May, K.; Ochsenfeld, C.; Öhm, H.; Schäfer, A.; Schneider, U.; Treutler, O.; von Arnim, M.; Weigend, F.; Weis, P.; Weiss, H. *Turbo Mole−Program System for ab initio Electronic Structure Calculations,* Version 5.2; Universität Karlsruhe: Karlsruhe, Germany, 2000.

(26) Perdew, J. P. *Phys. Rev. B* **1986**, *33*, 8822.

(27) Becke, A. D. *J. Chem. Phys.* **1988**, *84*, 4524.

(28) Baerends, E. J.; Ellis, D. E.; Ros, R. *Chem. Phys.* **1973**, *2*, 41. (b) Dunlap, B. I.; Connolly, J. W. D.; Sabin, J. R. *J. Chem. Phys.* **1979**, *78*, 3369. (c) Vahtras, O.; Almlöf, J. E.; Feyereisen, M. W.; *Chem. Phys. Lett.* **1993**, *213*, 514. (d) Eichkorn, K.; Treutler, O.; Öhm, H.; Häser, M.; Ahlrichs, R. *Chem. Phys. Lett.* **1995**, *242*, 652. (e) Eichkorn, K.; Weigend, F.; Treutler, O.; Ahlrichs, R. *Theor. Chem. Acc.* **1997**, *97*, 119.

(29) Schäfer, A.; Horn, H.; Ahlrichs, R. *J. Chem. Phys.* **1992**, *97*, 2571.

was used for all atoms except for the axial ligands X, the sulfurs, and the central iron which were described with a more accurate polarized triple-ζ valence (TZVP) basis.[30] The TurboMole multigrid m3 was used for the numerical integration of the exchange correlation energy and potential.[31] The energy was converged to 10^{-7} Hartree (Eh) and the convergence tolerances in the geometry optimization were 10^{-3} Eh/Bohr for the gradient and 10^{-6} Eh for the total energy.
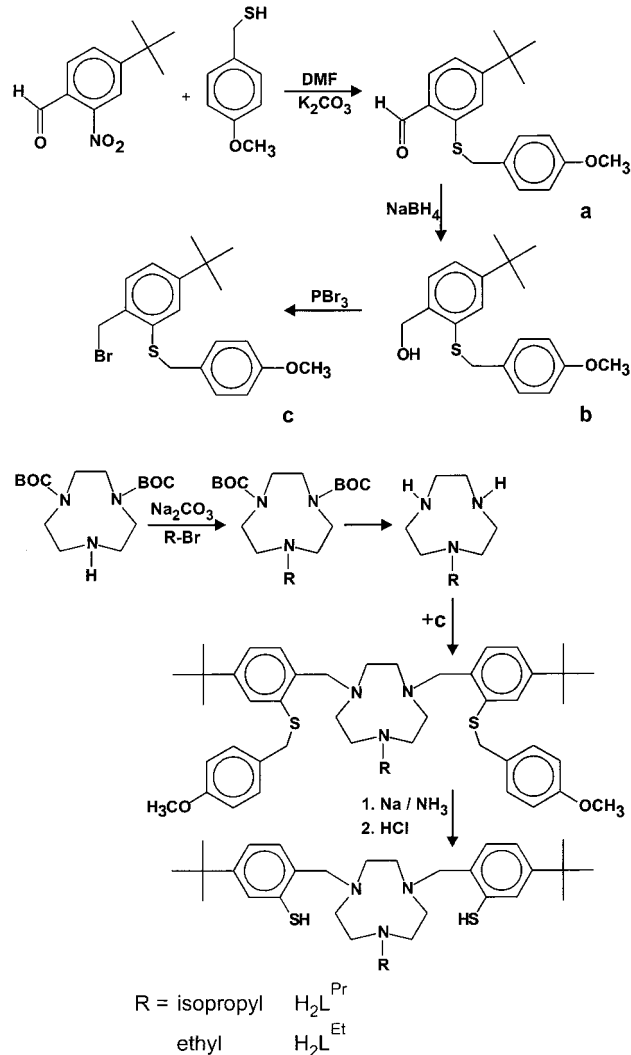
Single point calculations with the B3LYP functional[32] were carried out at the optimized geometries with the ORCA electronic structure package[33] that was also used to predict EPR[34] and Mössbauer[35] spectral parameters. For the quadrupole moment of ^{57}Fe, the value 0.16 barn was used.[36] In these calculations, the same basis sets were used as in the geometry optimization except for the iron basis which was based on the TZVP basis but with added steep s-functions and enhanced flexibility in the core region.[35] Special care was taken in the numerical integration procedure to accurately integrate the electron density in the core region as is required for the prediction of Mössbauer isomer shifts.[35] In addition, the iron basis contained two polarizing p-functions with Wachters exponents[37] and one additional f-function from the TurboMole library with exponent 2.5.[38] For the analysis of the bonding in the complexes, the canonical Kohn–Sham orbitals were localized according to the Pipek–Mezey criterion[39] and visualized through the interface of ORCA to the gOpenMol program.[40]

Physical Measurements. The apparatus used for the electrochemical experiments, magnetochemistry, and IR, UV–vis, EPR, and Mössbauer spectroscopy has been described in ref 6 as have the programs used for the simulations.

Results and Discussion

Syntheses and Characterization of Ligands and Complexes. Scheme 2 displays the synthetic routes employed for the preparation of the pendent arm macrocycles H_2L^{Pr} and H_2L^{Et}. The reaction of 2 equiv of 2-*tert*-butoxycarbonyl-oxyimino-2-phenylacetonitrile (BOC-ON) with 1,4,7-triazacyclononane in CHCl$_3$ yields [1,4,7]-triazonane-1,4-dicarboxylic acid di-*tert*-butylester in good yields[22] which reacts at the remaining unprotected secondary amine function with isopropylbromide or ethylbromide. After removal of the protecting BOC groups, the resulting *N*-isopropyl-1,4,7-triazacyclononane or *N*-ethyl-1,4,7-triazacyclononane reacts with 2 equiv of 1-bromomethyl-2-(4-methoxybenzylsulfa-nyl)-4-*tert*-butylphenyl (**c**, Scheme 2), respectively. In a final

(30) Schäfer, A.; Huber, C.; Ahlrichs, R. *J. Chem. Phys.* **1994**, *100*, 5829.
(31) Treutler, O.; Ahlrichs, R. *J. Chem. Phys.* **1995**, *102*, 346.
(32) (a) Becke, A. D. *J. Chem. Phys.* **1993**, *98*, 1372. (b) Becke, A. D. *J. Chem. Phys.* **1993**, *98*, 5648. (c) Becke, A. D. *J. Chem. Phys.* **1993**, *98*, 5648.
(33) Neese, F. *ORCA–an ab initio, DFT and Semiempirical Electronic Structure Package,* Version 2.1, Revision 78; Max-Planck-Institut für Strahlenchemie: Mülheim, Germany, October 2001.
(34) Neese, F. *J. Chem. Phys.* **2001**, *115*, 11080. (b) Neese, F. *J. Phys. Chem. A.* **2001**, *105*, 4290.
(35) Neese, F. *Inorg. Chim. Acta*, in press.
(36) Dufek, P.; Blaha, P.; Schwarz, K. *Phys. Rev. Lett.* **1995**, *75*, 3545.
(37) Wachter, A. J. H. *J. Chem. Phys.* **1970**, *52*, 1033. (b) Hay, P. J. *J. Chem. Phys.* **1977**, *66*, 4377.
(38) Basis sets were obtained from the ftp server of the quantum chemistry group at the University of Karlsruhe (Germany) under http://www.chemie.uni-karlsruhe.de/PC/TheoChem/.
(39) Pipek, J.; Mezey, P. G. *J. Chem. Phys.* **1989**, *90*, 4916.
(40) Laaksonen, L. *The gOpenMol effort*, Version 1.4; Espoo, Finland, 2000; obtained from http://www.csc.fi/~laaksone/gopenmol/gopen-mol.html.

Scheme 2. Ligand Synthesis

R = isopropyl H_2L^{Pr}
ethyl H_2L^{Et}

step, the protecting thioether groups were cleaved off in liquid NH$_3$ with Na, and the trishydrochloride salts [H$_2$L^{Et}]·3HCl and [H$_2$L^{Pr}]·3HCl were isolated, or alternatively, the corresponding air-sensitive sodium salts Na$_2$[L^{Et}] and Na$_2$-[L^{Pr}].

From the reaction of [H$_2$L^{Pr}]·3HCl and Zn(ClO$_4$)$_2$·6H$_2$O (1:1) in methanol, colorless crystals of [Zn^{II}(L^{Pr})] (**1**) were isolated after addition of 5 equiv of tetra-*n*-butylammoni-umhydroxide. The crystal structure shown later proves the dianionic ligand to be pentacoordinated forming a square base pyramidal polyhedron, ZnN$_3$S$_2$, with a secondary amine nitrogen in the apical position.

Similarly, the reaction of FeCl$_3$ with Na$_2$[L^{Et}] in methanol produces a bluish-green microcrystalline material of [Fe^{III}-(L^{Et})Cl] (**2**). The EI mass spectrum displays a peak at $m/z = 567$ which corresponds to the [Fe(L^{Et})]$^+$ cation. The effective magnetic moment of 5.9 μ_B at ambient temperature is indicative of a high spin ferric ion. In agreement with this notion, the zero-field Mössbauer spectrum displays a single quadrupole doublet at 80 K with isomer shift and quadrupole splitting parameters typical for octahedral high spin ferric complexes (Table 2). The electronic spectrum displays two S → Fe^{III} charge-transfer bands in the visible at 765 nm

Table 2. Zero-Field Mössbauer Parameters of Complexes **2**−**7** at 80 K

complex	δ^a, mm s^{-1}	$|\Delta E_Q|^b$, mm s^{-1}	S^c
2	0.49	0.63	$5/2$
3	0.44	0.78	$5/2$
4	0.47	1.00	$5/2$
5	0.26	2.82	$1/2^d$
	0.26	0.94	$1/2^e$
6	0.29	3.02	$1/2$
7	0.38	0.56	$1/2$ (58(2)%)
	0.55	1.42	$3/2$ (42(2)%)

^{a} Isomer shift vs α-Fe at 295 K. Typical errors are ±0.02 mm s^{-1} for δ and ±0.03 mm s^{-1} for ΔE_Q. ^{b} Quadrupole splitting. ^{c} Spin ground state. ^{d} [L^{Et}Fe−C≡N]. ^{e} [L^{Et}Fe−N≡C].

($\epsilon = 3.8 \times 10^3$ L mol^{-1} cm^{-1}) and 675 nm (3.4×10^3) which closely resemble those observed in [Fe^{III}(L^S)] where (L^S)$^{3-}$ is the trianion of 1,4,7-tris(4-*tert*-butyl-2-mercaptobenzyl)-1,4,7-triazacyclononane.[41,42]

Complexes [Fe^{III}(L^{Et})(OCH$_3$)]·CH$_3$OH (**3**) and [Fe(L^{Pr})-(OCH$_3$)]·CH$_3$OH (**4**) have been prepared from methanol/sodium methoxide solutions of the respective ligand and [Fe^{III}(acac)$_3$] (acac$^-$ = acetylacetonate(1−)) as deep blue microcrystals. Both compounds **3** and **4** each display a single quadrupole doublet at 80 K in the zero-field Mössbauer spectrum. The Mössbauer parameters (Table 2) are again indicative of octahedral high spin ferric ions ($S = 5/2$) as are the temperature independent magnetic moments at 5.9 μ_B.

The sixth coordination site in complexes containing the Fe^{III}(L^{Et})$^+$, or Fe^{III}(L^{Pr})$^+$, fragment can also be occupied by a cyanide ligand yielding the mononuclear neutral species [Fe^{III}(L^{Et})(CN)] (**5**) and [Fe^{III}(L^{Pr})(CN)] (**6**). These two complexes were obtained from the reaction of the respective macrocyclic ligand, [Fe(acac)$_3$] (1:1), and KCN or [NEt$_4$]-CN in methanol as green microcrystalline materials. Slow recrystallization of the crude product of **5** at 20 °C from toluene/CH$_2$Cl$_2$ (1:1) mixtures yielded single crystals of **5**·0.5 toluene·CH$_2$Cl$_2$ suitable for X-ray crystallography. In the IR spectrum of recrystallized **5** and crude **6**, a single ν(C≡N) stretching frequency is observed at 2095 and 2088 cm^{-1}, respectively. In addition, both species each exhibit a single quadrupole doublet in the zero-field Mössbauer spectrum at 80 K (Table 2) with very similar parameters. Since we have determined the crystal structure of recrystallized **5** (see later), it follows that these compounds contain a linear Fe−C≡N moiety.

Interestingly, the Mössbauer spectrum recorded at 80 K of crude **5** which was rapidly precipitated from the mother liquid (product C, Experimental Section) displays two quadrupole doublets as shown in Figure 1, spectrum C, in the ratio 60:40. When this material was recrystallized at −40 °C, the spectrum of the resulting material B shows an 80:20 ratio of the two species. Recrystallization at 20 °C from toluene/CH$_2$Cl$_2$ produced crystals A of almost pure [Fe(L^{Et})-(CN)] (**5**) (Figure 1, spectrum A).

Interestingly, the IR spectra of products A, B, and C differ also. The spectrum of pure A displays a single ν(C≡N)

(41) Beissel, T.; Bürger, K.-S.; Voigt, G.; Wieghardt, K.; Butzlaff, C.; Trautwein, A. X. *Inorg. Chem.* **1993**, *32*, 124.

(42) Butzlaff, C.; Bill, E.; Meyer, W.; Winkler, H.; Trautwein, A. X.; Beissel, T.; Wieghardt, K. *Hyperfine Interact.* **1994**, *90*, 453.
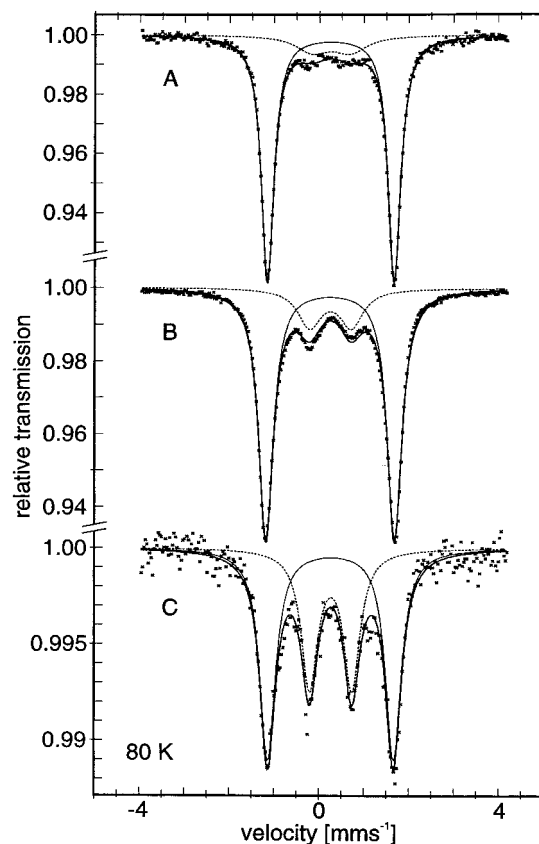
Figure 1. Zero-field Mössbauer spectra at 80 K of different preparations of solid **5**. Spectrum C, crude product as precipitated from the reaction mixture; spectrum B, from CH$_2$Cl$_2$ at −40 °C rapidly recrystallized material; spectrum A, from CH$_2$Cl$_2$ at 4 °C very slowly recrystallized material (needles which were used for the crystal structure determination). The lines represent the result of a fit with two Lorentzian doublets (- - - subspectrum of [L^{Et}Fe−N≡C]; — subspectrum of [L^{Et}Fe−C≡N]).

stretching frequency at 2095 cm^{-1} whereas those of B and C display two ν(C≡N) frequencies at 2095 and 2050 cm^{-1}. The intensity of the latter mode increases on going from B to C. We propose that this species with the ν(C≡N) frequency at 2050 cm^{-1} and Mössbauer parameters $\delta = 0.26$ mm s^{-1} and small quadrupole splitting of 0.94 mm s^{-1} at 80 K correspond to the isocyano isomer [Fe^{III}(L^{Et})(NC)].[43]

Both **5** and **6** are low spin ferric complexes. From temperature dependent magnetic susceptibility measurements of **5**, a temperature independent magnetic moment of 1.9 μ_B (20−300 K) has been determined. The X-band EPR spectrum of a frozen CH$_2$Cl$_2$ solution of **6** at 4 K displays a rhombic signal $g = (2.35(2), 2.19(2), 2.02(1))$. Note that all three g-values are >2.0. This behavior is also reflected in the large components of the magnetic hyperfine coupling as was determined from magnetic Mössbauer spectra (Table 3; Figure S1).

When pure NO gas was passed through an argon purged blue CH$_2$Cl$_2$ solution of **4**, a color change to purple-red was observed. Addition of *n*-hexane initiated the precipitation of red-black microcrystalline [Fe(L^{Pr})(NO)]·2.5CH$_2$Cl$_2$ (**7**) in low yield. The infrared spectrum recorded at 20 °C displays a broad ν(NO) stretching frequency at 1682 cm^{-1} typical for an {Fe−NO}^{7} nitrosyl complex.
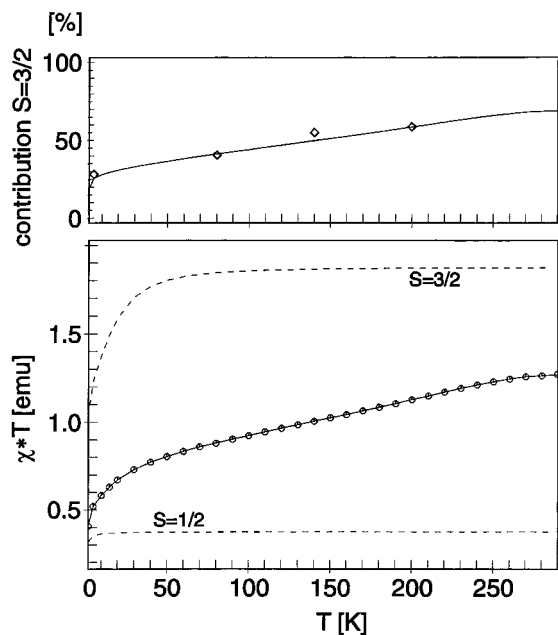
(43) Fehlhammer, W. P. *Chem. Rev.* **1993**, *93*, 1243.

Figure 2. Magnetic susceptibility data of solid **7** as a function of temperature (bottom), and deconvolution of the data into $S = \frac{1}{2}$ and $\frac{3}{2}$ contributions and the calculated temperature dependence of the $S = \frac{3}{2}$ contribution (top). The dashed lines represent the "basis set" of a pure $S = \frac{1}{2}$ ($g = 2$, $\theta_w = -0.3$ K) and $S = \frac{3}{2}$ ($g = 2$, $D = 20$ cm^{-1}) simulation, respectively (for convenience, the parameters were set to fixed values). The open diamonds in the top plot represent relative intensities of $S = \frac{3}{2}$ subspectrum in the corresponding zero-field Mössbauer spectrum (uncorrected for differences in the Lamb−Mössbauer factor).

Figure 2 (bottom) shows the temperature dependent magnetic susceptibility data as $\chi_M \cdot T$ versus T plot of **7**. The experimental data are corrected for underlying diamagnetism, temperature independent paramagnetism ($\chi_{TIP} = 4 \times 10^{-4}$ emu), and an unknown impurity ($S = \frac{5}{2}$; 10% abundance as estimated from the Mössbauer spectra of this sample). The dashed lines represent calculated expectation values for a pure $S = \frac{1}{2}$ and $\frac{3}{2}$ species, respectively, by using the following parameters: (for $S = \frac{1}{2}$) $g = 2.0$, $\theta_{Weiss} = -0.3$ K; and (for $S = \frac{3}{2}$) $g = 2.0$, $|D| = 20$ cm^{-1}. The contributions were then fitted to the experimental values by assuming a temperature dependent distribution of the $S = \frac{1}{2}$ and $S = \frac{3}{2}$ species. The solid line of the upper plot in Figure 2 gives the percentage of the $S = \frac{3}{2}$ species as a function of the temperature where the open diamonds represent experimental values obtained from zero-field Mössbauer spectra at the respective temperature.

Figure 3 displays the zero-field Mössbauer spectrum of **7** at 200 K. Clearly, two quadrupole doublets are observed at isomer shifts of 0.35 and 0.49 mm s^{-1} and quadrupole splitting parameters of 0.46 and 1.35 mm s^{-1}, respectively. The former corresponds to the $S = \frac{1}{2}$ and the latter to the $S = \frac{3}{2}$ species (ratio 41:59, in excellent agreement with the data in Figure 2).

The applied-field (4 and 7 T), variable temperature (4.2 and 120 K) Mössbauer spectra of **7** are shown in Figure 4, and Table 3 gives the spin-Hamiltonian parameters obtained from a fit of the spectra to the two species $S = \frac{1}{2}$ and $S = \frac{3}{2}$. It is noteworthy that the complex [LFe(NO)(N$_3$)$_2$] $S = \frac{3}{2}$ displays similar isomer shift (0.62 mm s^{-1}), quadrupole
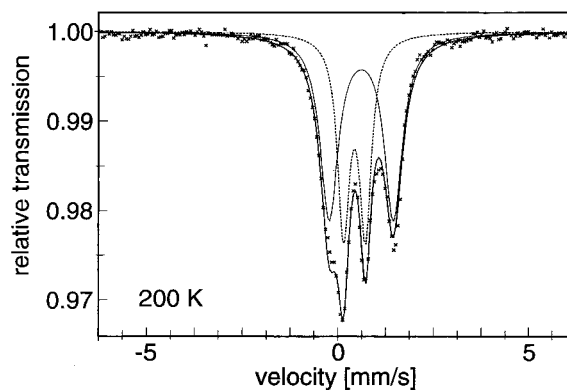
Figure 3. Zero-field Mössbauer spectrum of solid **7** recorded at 200 K and simulation for two subspectra ($\cdots$ subspectrum of the $S = \frac{1}{2}$ species; — subspectrum of the $S = \frac{3}{2}$ isomer) (for parameters, see text).
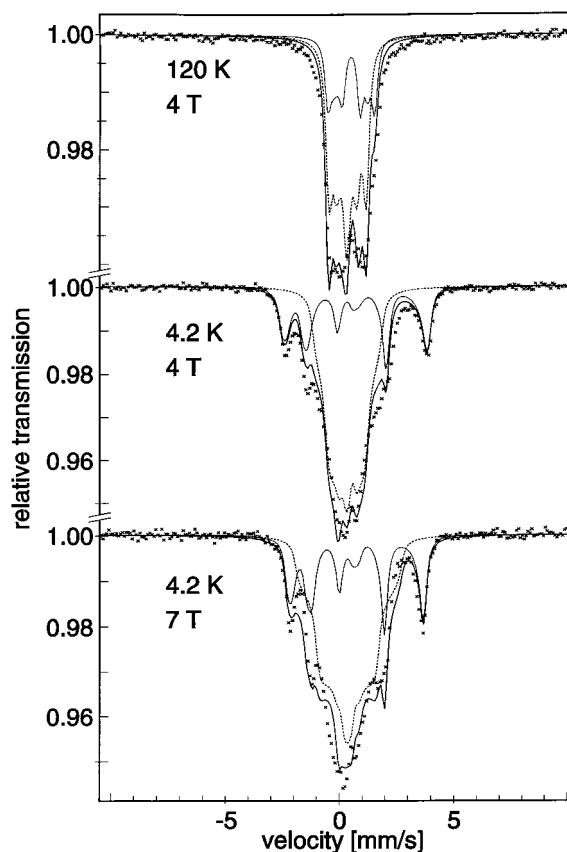

Figure 4. Applied field Mössbauer spectra of solid **7** at 120 and 4.2 K. The 4.2 K data are corrected for a ~10% background of a widely split, broad six-line pattern (± 8 mm s^{-1}) due to a high spin ($S = \frac{5}{2}$) contamination. The dashed and solid lines represent spin-Hamiltonian simulations for the $S = \frac{1}{2}$ and $S = \frac{3}{2}$ species, respectively. Parameters are given in Table 3. The simulation for the $S = \frac{1}{2}$ species is obtained in the limit of fast relaxation whereas the spectrum of the $S = \frac{3}{2}$ species shows slow relaxation at 4.2 K.

splitting (-1.28 mm s^{-1}), asymmetry parameter ($\eta = 0.2$), zero-field splitting parameters ($D = +13.6$ cm^{-1}, $E/D = 0$), and ^{57}Fe A-tensor components/g$_N\beta_N$ (-21.3, -20.8, -25.4) T.[6] This complex has been shown by Solomon et al.[16,17] and our group[6] to be best described as high spin ferric ($S_{Fe} = \frac{5}{2}$) coupled antiferromagnetically to NO$^-$ ($S_{NO} = 1$). Strikingly similar are the Mössbauer parameters for the octahedral complex [cis-(cyclam)Fe(NO)I]$^+$ ($S = \frac{3}{2}$)[6] where $E/D_{3/2} < 0.01$ and $\eta = 0.4$. We propose that the $S = \frac{3}{2}$

Electronic Structure of Octahedral Iron Complexes

Table 3. Spin-Hamiltonian and Hyperfine Parameters of Compounds **4**, **6**, **7**, and [Fe(pyS₄)(NO)] Obtained at Liquid Helium Temperatures

	4	**6**	**7**	**7**	**[Fe(pyS₄)(NO)]**
S	$^5/_2$	$^1/_2$	$^1/_2$	$^3/_2$	$^1/_2$
δ, mm s^{-1}	0.46(2)	0.29(2)	0.38(2)	0.55(2)	0.33(2)
ΔE_Q, mm s^{-1}	−1.01(2)	−3.01(3)	−0.63(4)	−1.35(4)	−0.40(3)
η	0.6(1)	0.2(2)	0.8(2)	0(0.1)	0.3(3)
α, β, γ (deg) (Euler angles)	90, 90, 0	71, 54, 0^a		0, 24(5), 0^b	
g_1	2.0	2.35(2)	2.07(2)	2	2.03(1)
g_2	(isotropic)	2.19(2)	2.02(1)	2	2.01(1)
g_3		2.02(1)	1.99(2)	2	1.96(1)
D, cm^{-1}	0.45(10)			16(4)	
E/D	0.33^d			0^c	
$A_x/g_N\beta_N$, T	−17.8(3)	−60(1)^e	−14.7(10)	−19.6(4)	−7.7(25)
$A_y/g_N\beta_N$, T	−18.0(3)	−8(6)	−15.5(10)	−19.6(4)	+5.8(25)
$A_z/g_N\beta_N$, T	−22.9(3)	−42(2)	+17.9(10)	−25.4(15)	−10.3(25)

^{a} Euler angles are obtained from a fitting procedure by using a genetic algorithm. The result is not an unique solution due to the relatively poor approximation of the experimental data and an ambiguity problem of general efg rotations; e.g. a good fit is also obtained with α, β, γ = 60, 40, 33.
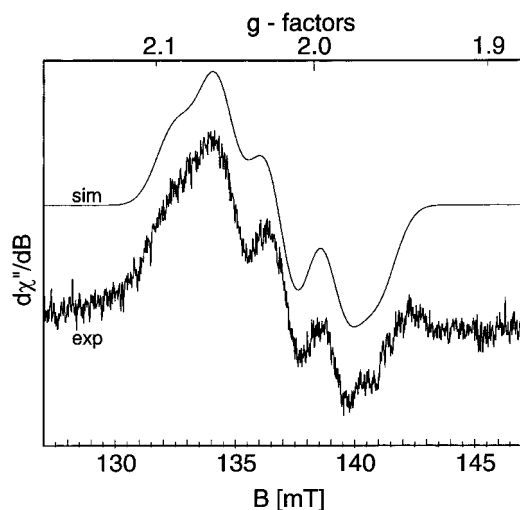

Figure 5. S-Band EPR spectrum of **7** in dimethylformamide solution (∼1 mM). Experimental conditions: 3.8710 GHz microwave frequency, 2.1 μW power, 0.43 mT (100 kHz) modulation, temperature 6 K. The solid line is a simulation with g = (2.064, 2.018, 1.986) and A = (15.6, 20.6, 16.6) × 10^{-4} cm^{-1} (linear approximation for the hfs) as given in the text and with Gaussian line widths W = (2, 2, 1.6) mT.
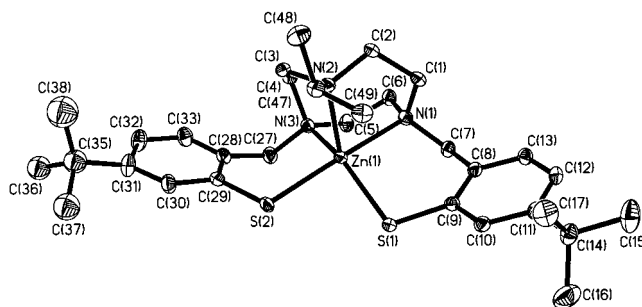

Figure 6. Structure of the neutral molecule [ZnL^{Pr}] in crystals of **1**·1.5CH₂-Cl₂.
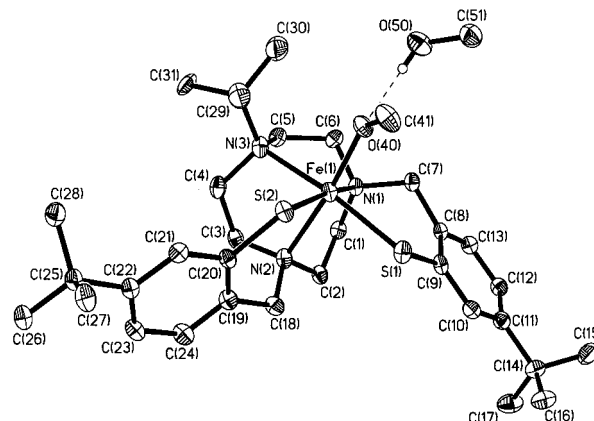
Figure 7. Structure of the neutral molecule [Fe^{III}L^{Pr}(OCH₃)] in crystals of **4**·CH₃OH.

form of complex **7** should also be described as high spin ferric ($S = {}^5/_2$) coupled antiferromagnetically to NO$^-$ ($S = 1$). The rhombicity of **7** ($S = {}^3/_2$) may well be a feature introduced by the steric requirements of the coordinated ligand (L^{Pr})$^{2-}$ (see later).

Figure 5 exhibits the S-band EPR spectrum of **7** ($S = {}^1/_2$) dissolved in dimethylformamide (∼1 mM) at 6 K. A rhombic signal is observed at g_1 = 2.07, g_2 = 2.02, g_3 = 1.99 with hyperfine splitting to one nitrosyl nitrogen: $A_1(^{14}N)$ = 10(4) × 10^{-4} cm^{-1} (30 MHz), $A_2(^{14}N)$ = 21(2) × 10^{-4} cm^{-1} (63 MHz), $A_3(^{14}N)$ = 14(4) × 10^{-4} cm^{-1} (42 MHz). The above frozen solution EPR spectrum also does not exhibit a signal due to an $S = {}^3/_2$ species.

Crystal Structure Determinations. The structures of complexes **1**, **4**, **5**, and **7** have been determined by single-crystal X-ray crystallography. Figures 6−9 display the structure of the respective neutral molecule in crystals of **1**, **4**, **5**, and **7**, respectively, and Table 4 gives selected bond distances and angles of the respective iron coordination polyhedron.

The neutral molecule [L^{Pr}Zn] in crystals of **1** (Figure 6) shows the zinc ion to be in a square-based pyramidal

environment of three amine nitrogen and two thiolatosulfur atoms.

Similarly, the iron(III) ion in the neutral molecule [L^{Pr}-Fe(OCH₃)] (Figure 7) in crystals of **4** is in a distorted octahedral environment consisting of the pentadentate ligand (L^{Pr})$^{2-}$ and a methoxy ligand in the sixth position. The observed Fe−N and an Fe−S bond distances are long and consistent with the high spin electronic configuration of the central ferric ion ($S = {}^5/_2$). Interestingly, the Fe−O−CH₃ group is bent (Fe−O−C 123.2(2)°), and the Fe−O bond at 1.901(2) Å is relatively short, indicating some multiple bond character. The oxygen donor atom of the coordinated methoxy group is also involved in a hydrogen bond to a methanol molecule of crystallization (O(40)···O(50) 2.788(6) Å).
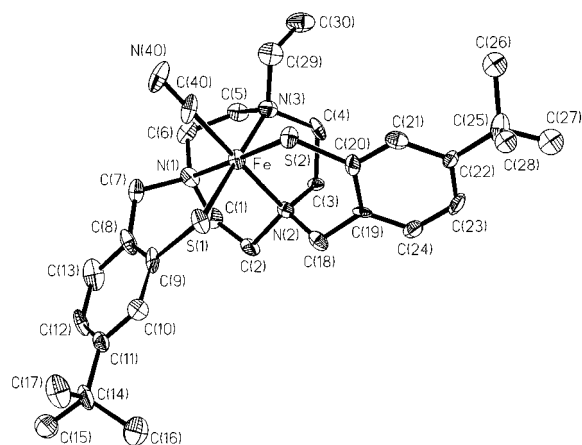
Figure 8. Structure of the neutral molecule [FeL^{Et}(CN)] in crystals of **5**·0.5C$_6$H$_5$CH$_3$·CH$_2$Cl$_2$.
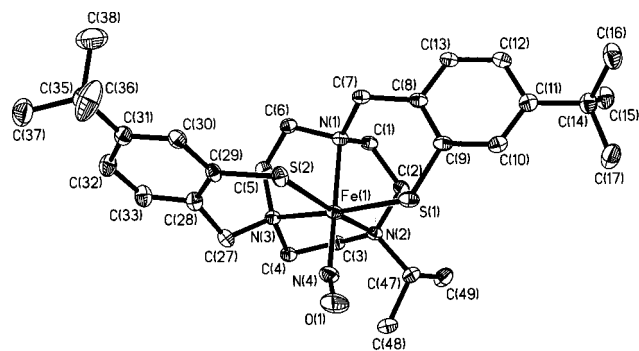
Figure 9. Structure of the neutral molecule [FeL^{Pr}(NO)] in crystals of **7**·2.5CH$_2$Cl$_2$.

The neutral molecules in crystals of **5** comprise a ferric ion coordinated to a pentadentate dianionic ligand (L^{Et})$^{2-}$ and a coordinated cyanide anion in the sixth position. The Fe—N and Fe—S bonds are significantly shorter than corresponding ones in **4**; they are in excellent agreement with the fact that the ferric ions in **5** possess a low spin electron configuration ($S = \frac{1}{2}$). The Fe—C≡N group is nearly linear.

Crystals of **7** consist of the neutral mononuclear species [L^{Pr}Fe(NO)], where the pentadentate dianion (L^{Pr})$^{2-}$ and a nitrosyl group are coordinated to an iron ion. As was shown by temperature dependent magnetic susceptibility and Mössbauer spectroscopy, the complex exists at 100 K in the solid state of an approximately 50:50 mixture of an $S = \frac{1}{2}$ and an $S = \frac{3}{2}$ species. We will show that the $S = \frac{1}{2}$ species is best described as low spin ferrous with a coordinated nitrosyl radical, Fe^{II}(·NO), whereas the $S = \frac{3}{2}$ species is probably a high spin ferric species coordinated to NO$^-$ ($S = 1$). If this is true, one might expect the sum of the four Fe—N1, Fe—N3, Fe—S1, and Fe—S2 bond lengths in **7**, which is 9.333 Å in **4** and 8.645 Å in **5**, to be close to the arithmetic average of the bond lengths in **4** and **5**. This is indeed the case; the experimental sum in **7** is 9.041 Å which is very close to the calculated average of **4** and **5** at 8.99 Å. The fact that **7** contains then a low spin ferrous ion (50%) whereas **5** contains a low spin ferric ion does not impede the argument. Equivalent bonds in octahedral low spin ferric and low spin ferrous complexes are often very similar.

Table 4. Selected Bond Distances (Å) and Angles (deg)

Complex [**1**]·1.5CH$_2$Cl$_2$			
N1—Zn	2.262(3)	S1—C9	1.765(4)
		S2—C29	1.762(4)
N2—Zn	2.165(3)		
N3—Zn	2.164(3)	S1—Zn—S2	88.89(3)
S1—Zn	2.333(1)	S2—Zn—N3	93.5(1)
S2—Zn	2.399(1)	N3—Zn—N1	80.9(1)
		N1—Zn—S1	92.6(1)
Complex [**4**]·CH$_3$OH			
O40—Fe	1.901(2)	S1—C9	1.770(3)
N1—Fe	2.202(2)	S2—C20	1.766(3)
N2—Fe	2.275(2)	O40—C41	1.418(3)
N3—Fe	2.353(2)		
S2—Fe	2.368(1)	C41—O40—Fe	123.2(2)
S1—Fe	2.410(1)	S1—Fe—S2	90.99(3)
		S2—Fe—N3	97.73(6)
		N3—Fe—N1	78.35(8)
		N1—Fe—S1	91.11(6)
Complex [**5**]·0.5toluene·CH$_2$Cl$_2$			
N1—Fe	2.034(9)	S1—C9	1.763(13)
N2—Fe	2.063(8)	S2—C20	1.736(12)
N3—Fe	2.119(10)	C40—N40	1.147(14)
S1—Fe	2.303(4)		
S2—Fe	2.192(4)	N40—C40—Fe	177.1(10)
C40—Fe	1.911(13)		
Complex [**7**]·2.5CH$_2$Cl$_2$			
N1—Fe	2.191(2)	S1—C9	1.768(3)
N2—Fe	2.274(2)	S2—C29	1.764(3)
N3—Fe	2.151(2)	O1—N4	1.182(3)
S1—Fe	2.304(1)		
S2—Fe	2.395(1)	O1—N4—Fe	147.0(2)
N4—Fe	1.749(2)		

It is significant that the two M—S bonds in all present structures, including **1**, are significantly different, as are the two Fe—N bonds in trans positions relative to these M—S bonds. The *longer* M—S bond is always in the trans position relative to the *longer* Fe—N bond. The difference, Δ, between the sum of the long Fe—S and the long Fe—N distance and the sum of the short Fe—S and short Fe—N distance is nearly constant: Δ in **1** is 0.164 Å; in **4**, it is 0.193 Å; in **5**, 0.196 Å; and in **7**, it is 0.214 Å. This is believed to be a steric effect of the coordinated macrocyclic ligand rather than an electronic effect of the individual transition metal ion.

Mössbauer Spectra of [Fe^{II}(pyS$_4$)X] Complexes (X = NO, CO, PR$_3$, SR$_2$). The octahedral complexes [Fe(NO)(pyS$_4$)] (**A**) ($S = \frac{1}{2}$) and [Fe(NO)(pyS$_4$)]BF$_4$ (**B**) ($S = 0$) of the {Fe—NO}^{7} and {Fe—NO}^{6} type,[7] respectively, are structurally similar to complex **7**. The ligand pyS$_4$ represents the pentadentate dianion 2,6-bis(2-mercaptophenylthiomethyl)pyridine(2−). Important structure and spectroscopic parameters of **A** and **B** are summarized in Table 6. Density functional calculations[7] have allowed the interpretation that the unpaired electron in **A** resides predominantly in a π* type NO orbital. This leads to a description of the electronic structure of **A** as low spin ferrous ($S_{Fe} = 0$) coordinated to an ·NO radical ($S_{NO} = \frac{1}{2}$) (see later).

Figure 10 displays the S-band EPR spectrum of **A** in a frozen dmf/CH$_2$Cl$_2$ mixture at 5 K. A rhombic $S = \frac{1}{2}$ signal is observed at $g_1 = 2.035$, $g_2 = 2.012$, $g_3 = 1.961$. The signal shows rhombic hyperfine splitting to two ^{14}N-nitrogen atoms: the larger hyperfine coupling constants at $A_1(^{14}N) = 11(1) \times 10^{-4}$ cm^{-1} (33 MHz), $A_2(^{14}N) = 13.3(10) \times 10^{-4}$ cm^{-1} (40 MHz), $A_3(^{14}N) = 6.7(10) \times 10^{-4}$ cm^{-1} (20 MHz)

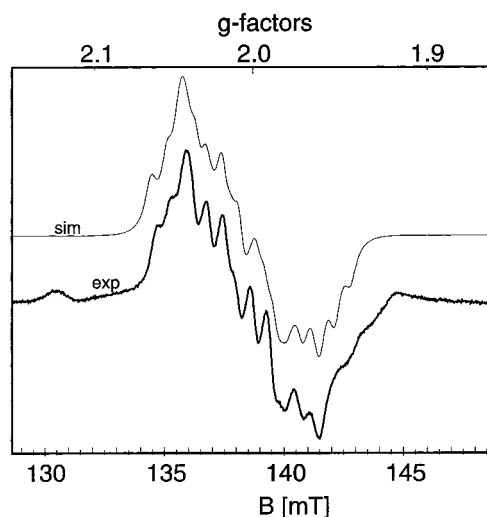**Figure 10.** S-Band EPR spectrum of [Fe(NO)(pyS$_4$)] (**A**) in frozen dmf/CH$_2$Cl$_2$ solution at 5 K. Experimental conditions: 3.8828 GHz microwave frequency; 170 nW power. See text for simulation parameters.

Table 5. Mössbauer Parameters at 80 K of [Fe^{II}(pyS$_4$)X] Complexes[a]

	δ, mm s^{-1} [b] exptl/DFT	ΔE_Q, mm s^{-1} [c] exptl/DFT	S[d]	η^e exptl/DFT
[Fe^{II}(pyS$_4$)]$_2$ (**C**)[f]	0.44/0.45	0.43 /−0.44	0	0.1(1)/0.61
[Fe^{II}(−NO)(pyS$_4$)] (**A**)	0.33/0.33	−0.40 /−0.63	$^1/_2$	0.3(3)/0.57
[Fe^{II}(PR$_3$)(pyS$_4$)] (**D**)[g]	0.34/0.39	0.69/+0.70	0	0.9(1)/0.16
[Fe^{II}(CO)(pyS$_4$)] (**E**)	0.19/0.20	0.88/+1.02	0	0.1(1) /0.03
[Fe^{II}(NO$^+$)(pyS$_4$)]$^+$ (**B**)	0.04/0.07	−1.63/2.07[h]	0	0.9(1)/0.72

[a] Second values are calculated by DFT methods; the experimental errors are typically +0.02 mm s^{-1} for δ and ΔE_Q and as indicated for η. [b] Isomer shift vs α-Fe at 298 K. [c] Quadrupole splitting. [d] Spin ground state. [e] Asymmetry parameter $|V_{xx} - V_{yy}|/|V_{zz}|$. [f] Experimental values are for a dinuclear species [Fe^{II}(pyS$_4$)]$_2$ containing two μ-thiolato bridges (Blum, N.; Sellmann, D. Unpublished results). The DFT calculations were carried out for the hypothetical mononuclear species [Fe^{II}(pyS$_4$)(S(CH$_3$)$_2$)]. [g] The complex [Fe^{II}(pyS$_4$)(P(CH$_3$)$_3$)] has been investigated (Blum, N.; Sellmann, D. Unpublished results); the calculations are for [Fe(pyS$_4$)(PH$_3$)]. [h] The experimental negative sign is not well defined at an asymmetry parameter η of 0.94.

are assigned to the coordinated nitrosyl nitrogen whereas the smaller ones at $A_1(^{14}N) = 6.4(10) \times 10^{-4}$ cm^{-1} (19 MHz), $A_2(^{14}N) = 3.4(10) \times 10^{-4}$ cm^{-1} (10 MHz), $A_3(^{14}N) = 5.6(10) \times 10^{-4}$ cm^{-1} (17 MHz) are assigned to the pyridine ^{14}N hyperfine coupling. By using these parameters, an excellent fit of the experimental spectrum is obtained (Figure 10).

The zero-field Mössbauer spectra of **A** and **B** each display a single doublet at 80 K; the corresponding values of the isomer shift, δ, and quadrupole splitting, ΔE_Q, are summarized in Table 5. Interestingly, these parameters for the {Fe−NO}^{7} ($S = ^1/_2$) complex **A** and the $S = ^1/_2$ component of **7** (Tables 2, 3) are strikingly similar whereas they are remarkably different from those of the {Fe−NO}^{6} species **B**, the Mössbauer spectrum of which displays a doublet with a much smaller isomer shift of 0.04 mm s^{-1} and a large quadrupole splitting of $|\Delta E_Q| = 1.63$ mm s^{-1} at 80 K. Similarly, the octahedral {Fe−NO}^{6} species [L′Fe(NO)(ONO)(NO$_2$)](ClO$_4$) and *trans*-[Fe(cyclam)(NO)Cl]$^{2+}$ possess an isomer shift of 0.04 and 0.03 mm s^{-1}, respectively, and quadrupole splittings of 2.05 and 1.37 mm s^{-1}, respectively.[6] Thus, these Mössbauer parameters appear to be
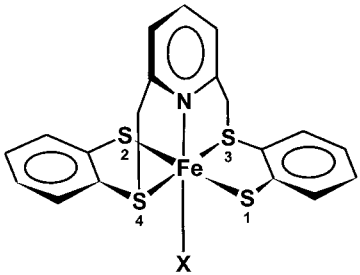
typical for octahedral {Fe−NO}^{6} species, and they are not very sensitive to the nature of the other donor atoms (i.e., nitrogen, oxygen, or sulfur).

Magnetic Mössbauer spectra of solid complex **A** reveal the presence of moderately strong hyperfine field at the Mössbauer nucleus due to spin density at the iron site. From a spin-Hamiltonian simulation of the spectra recorded at 1, 4, 7 T and temperatures in the range 4.2−120 K (Figure S2), the components of the magnetic hyperfine coupling tensor were determined to be A/g$_N\beta_N$ = (−7.7, 5.8, −10.4) T. The same analysis also yields the sign of the efg main component and the asymmetry parameter as given in Table 5. The isotropic part of the A tensor $^1/_3$ tr(**A**)/g$_N\beta_N$ = −4.1 T is unusually low with respect to that of typical "innocent" paramagnetic iron site ($\approx$16−22 T) or in comparison to the comparable nitrosyl complex *trans*-[Fe(cyclam)(NO)Cl]$^{2+}$ which has $^1/_3$ tr(**A**)/g$_N\beta_N$ = −8.4 T. Hence, the spin density at the iron site of **A** is exceptionally low. At the same time, the pronounced anisotropy in **A**$_{Fe}$ indicates strong dipolar contributions presumably because of the presence of high charge asymmetry in the magnetic orbitals.

Because the isomer shift difference between **A** and **B** is very large, $\Delta\delta$ = 0.29 mm s^{-1}, it is at first sight tempting to assume that the one-electron oxidation of the {Fe−NO}^{7} to the {Fe−NO}^{6} species is metal centered[6] rather than involving oxidation of the coordinated •NO to a coordinated NO$^+$, although this latter interpretation would be in excellent accord with the observation that the ν(NO) stretching frequency is observed at 1648 cm^{-1} in **A** but at 1893 cm^{-1} in **B**. If the Fe(II)(•NO) model is correct, one would have to conclude that the observed large change of the isomer shift on going from **A** to **B** is due to the differing π acceptor abilities of an •NO versus an NO$^+$ ligand. This interpretation had been strongly suggested by our DFT calculations (see later) on [Fe(pyS$_4$)X] complexes where X is a ligand of varying π acceptor strength.

To test this hypothesis experimentally, we have recorded the Mössbauer spectra of a series of complexes [Fe^{II}(pyS$_4$)X] where X is a bridging thiolato σ donor S-atom as in complex **C** (Table 5), a phosphine ligand with very moderate π acceptor capability (complex **D**), or a carbonyl ligand with strong π acceptor capability (complex **E**). As expected, **C** displays the largest isomer shift at 0.44 mm s^{-1} and smallest quadrupole splitting at 0.46 mm s^{-1} of the series in excellent agreement with the notion that **C** contains a spherical low spin ferrous ion (t$_{2g}^6$) octahedrally coordinated to six σ donor atoms. With increasing π acceptor strength of the single ligand X, the isomer shift decreases to 0.19 mm s^{-1} in the carbonyl complex **E**, and at the same time, the quadrupole splitting parameter, $|\Delta E_Q|$, increases to 0.78 mm s^{-1}. NO$^+$ is the strongest π acceptor, and consequently, the isomer shift of **B** is the smallest of the series at 0.04 mm s^{-1}, and $|\Delta E_Q|$ is the largest at 1.60 mm s^{-1}.

The appearance of the large quadrupole splitting indicates the presence of anisotropic covalent d-charge delocalization by the ligands. Similar phenomena have been described for other iron ions without a priori valence contributions to the efg, for example, Fe(III) high spin with a single oxo ligand

Table 6. Structural and Spectroscopic Data for Complexes [Fe^{II}(X)(pyS$_4$)] **A−E** and Calculated Data in Parenthesis

	A		**B**		**C**[b]		**D**		**E**	
Fe−X[a]	1.712	(1.705)	1.634	(1.640)		(2.340)	2.225	(2.223)	1.757	(1.753)
Fe−N[a]	2.167	(2.195)	2.005	(2.046)		(1.942)	2.011	(1.967)	2.014	(2.022)
Fe−S$_1$[a]	2.297	(2.322)	2.313	} (2.335)		} (2.331)	2.292	} (2.325)	2.311	} (2.325)
Fe−S$_2$[a]	2.301	(2.332)	2.256				2.305		2.289	
Fe−S$_3$[a]	2.300	(2.375)	2.254	} (2.284)		} (2.226)	2.204	} (2.233)	2.225	} (2.242)
Fe−S$_4$[a]	2.297	(2.275)	2.312				2.201		2.232	
α(Fe−N−O), deg	150.4[c] } (149.1)		179.5	(179.9)						
	143.8[c]									
ν(NO), cm^{-1} [d]	1648		1893							

[a] X = •NO(**A**), NO$^+$ (**B**), SR (**C**), PR$_3$ (**D**), CO (**E**). Bond lengths in Å. [b] Experimental values not available. [c] Disordered. [d] Experimental ν(NO) stretching frequency.

or Fe(III) $S = {}^3/_2$ in a square based pyramidal ligand field with strong equatorial ligands.[44]

This series demonstrates that a shift of the isomer shift of ∼0.4 mm s^{-1} can be observed in a structurally very similar series of complexes where only a single ligand varies in its π acceptor strength *without changing the formal oxidation state at the central metal ion (low spin Fe^{II}).*

Electronic Structure of Complexes [Fe(pyS$_4$)X]$^{0/1+}$. To obtain more insight into the results of the Mössbauer and EPR spectroscopic experiments, we have further characterized the complexes [Fe(pyS$_4$)(X)] (**C**, **D**, **E**) as well as the {Fe−NO}^{7} and {Fe−NO}^{6} complexes [Fe(pyS$_4$)(NO)]$^{0/+1}$ (**A**, **B**) by DFT methods. Selected calculated geometric parameters are compared to the corresponding experimental values in Table 6. In general, the calculations are in excellent agreement with the experimental structures. In particular, the bond distances to the axial ligands, X, are very well reproduced, and the effect of X on the pyridine nitrogen donor in trans position is also accurately predicted. For **A** and **B**, our results are in full agreement with the previously reported calculations.[7]

In addition to structural parameters, the Mössbauer isomer shift, δ, the quadrupole splitting parameters, ΔE_Q, and the asymmetry parameters, η, were calculated with the B3LYP DFT method. The results are shown together with the experimental data in Table 5. It is observed that the calculations lead to excellent agreement with the experimental numbers for the isomer shift (maximum error 0.05 mm s^{-1}) and good agreement with experiment for the quadrupole splitting. In particular, the experimentally observed trend in the isomer shift is fully reproduced by the calculations, that is, **B** < **E** < **A** ∼ **D** < **C**. We conclude from this result and the good agreement between calculated
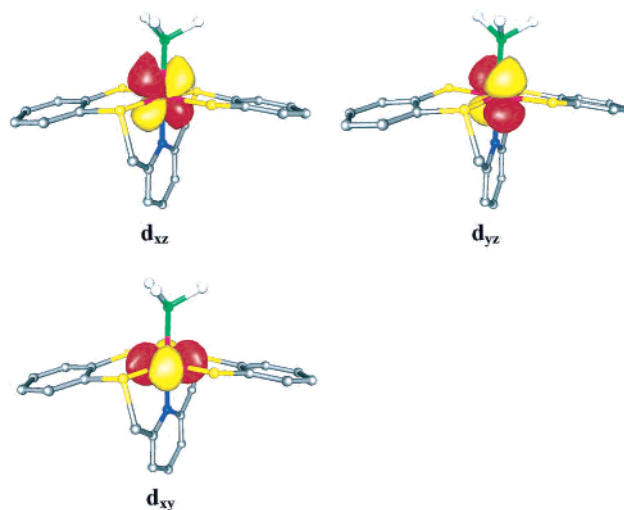

Figure 11. Low spin d^6 character of complexes [Fe(pyS$_4$)(X)], **A−E**, illustrated with complex **D** (X = PH$_3$). Shown are the three doubly occupied iron t$_{2g}$-based localized MOs.

and experimental structure parameters that the calculations faithfully describe their electronic structure.

Previously, it has been thought that a decrease of 0.15 mm s^{-1} of the isomer shift in going from {Fe−NO}^{7} ($S = {}^1/_2$) to {Fe−NO}^{6} ($S = 0$) reflects a metal centered oxidation.[6] However, we now believe that the present {Fe−NO}^{7} ($S = {}^1/_2$) and {Fe−NO}^{6} ($S = 0$) species are best described as nitrosyl complexes containing a low spin Fe(II) ion bound to NO• and NO$^+$, respectively. This conclusion is supported by the calculations: The analysis of the Kohn−Sham wave function in terms of localized MOs (LMOs; Figure 11) shows that in the species **B−E** there are three doubly occupied LMOs that are dominantly localized on the iron center and that derive from t$_{2g}$ orbitals in the octahedral limit. Furthermore, closely above the HOMO, there are two unoccupied orbitals that derive from the e$_g$ orbitals in the octahedral limit (not shown). This result strongly suggests that the description

(44) Westcott, B. L.; Enemark, J. H. In *Inorganic Electronic Structure and Spectroscopy*; Solomon, E. I., Lever, A. B. P., Eds.; Wiley: New York, 1999; Vol. II, p 403.
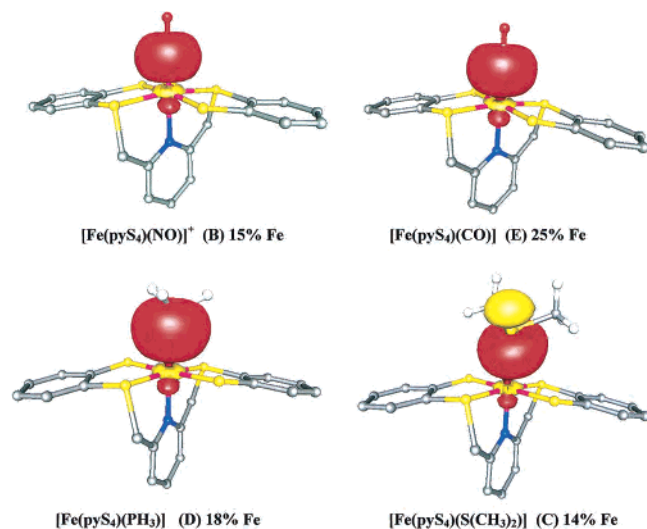
Figure 12. Comparison of σ bonding interactions in complexes **B**−**E**. Shown are the doubly occupied localized Fe−X σ bonding MOs which are dominantly ligand based.

Figure 13. Comparison of π back-bonding interactions in complexes **B**−**E**. Shown are the doubly occupied localized Fe-d$_\pi$−ligand-π*orbitals.

of **A**−**E** in terms of a central iron ion in the low spin d^6 ($S = 0$) configuration applies. While the result would have been anticipated for complexes **C**, **D**, **E**, the case of the NO complexes **A** and **B** has frequently been regarded as "special" with no limiting valence structure being appropriate.[44]

We have also searched for other solutions to the Kohn−Sham equations that would correspond to electronic situations such as Fe(IV) ($S_{Fe} = 1$) antiferromagnetically coupled to NO$^-$ ($S_{NO^-} = 1$) or low spin Fe(III) ($S_{Fe} = {}^1\!/_2$) antiferromagnetically coupled to NO$^\bullet$ ($S_{NO} = {}^1\!/_2$), but they either do not appear to exist or are much higher in energy than the low spin d^6 solutions.

While we have stressed the formal similarities between complexes **B**−**E**, there are also some pronounced differences which are related to the σ bonding and π back-bonding capabilities of ligand X. Again, these can be conveniently analyzed in terms of LMOs.

Figure 12 shows the bonding σ interactions between the lone pairs on ligand X and the central iron ion. In all cases, it is observed that there is a bonding interaction with the iron d$_{z^2}$ derived orbital which amounts to ≈15% iron character except for the CO complex where it is significantly higher (≈25%).

In Figure 13, the occupied π LMOs from the iron t$_{2g}$ based orbitals are shown. It is evident that for **B** these π orbitals have a rather large admixture of ligand character (≈70% Fe and 30% NO). In addition, the interaction between the central iron and the π* orbital of the NO ligand is seen to be *bonding* (constructive overlap). This signifies a very strong back-bonding interaction between the low spin Fe(II) and an NO$^+$ ligand. A similar situation exists for the CO complex **E** where also a large back-bonding interaction is observed, which is, however, somewhat weaker (≈80% Fe and 20% CO-π*) than for the NO$^+$ complex. The other two complexes **C** and **D** show much less π back-bonding capability with iron characters of >90% in the π orbitals. Thus, neither the phosphine nor the thioether is a good π acceptor with Fe(II).
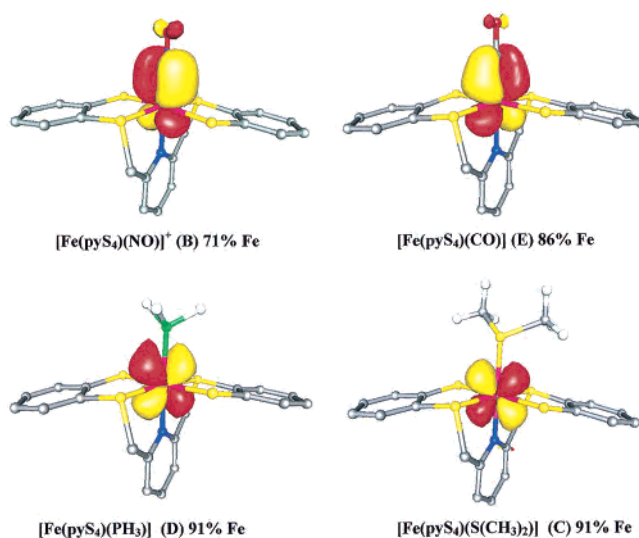
Electronic Structure of {Fe−NO}^{7} (A). Spin unrestricted DFT calculations were carried out for the paramagnetic complex **A**. As observed for the diamagnetic complexes **B**−**E**, the optimized structure is in good agreement with the experimental values and also with previous calculations for the same complex.[7] The calculated Mössbauer parameters show excellent agreement with experiment (Table 5) which indicates that the electron distribution in **A** is well described by the present calculations. The g-values calculated using the methodology given in ref 34a also support the electronic structure description of **A** (see later). At the B3LYP level, values of 2.015, 1.991, and 1.949 are obtained, while at the BP86 level, g-values of 2.014, 2.002, and 1.964 are calculated. Both sets are in good agreement with experiment (Figure 10) and support the notion of a mainly NO-π* centered SOMO in **A** which leads to relatively limited spin−orbit coupling (SOC) in the ground state due to small SOC constants of N and O.

In analogy with complexes **B**−**E**, the analysis of the localized Kohn−Sham MOs shows that there are six electrons in occupied orbitals that are dominantly localized on the iron (not shown) defining thereby the low spin d^6 configuration also for **A**. The singly occupied natural orbital of **A** is shown in Figure 14. The density of this orbital dominates the spin density distribution which, according to the B3LYP method, is localized ~33% on the d$_{z^2}$ orbital of the central iron and ~66% in a π* orbital of the NO ligand. Furthermore, the interaction between the two orbitals is seen to be bonding from Figure 12 which indicates that the interaction arises from the lower lying singly occupied π* orbital of the NO ligand with the higher lying empty orbital localized on the iron center. We describe this interaction therefore as a σ charge donation from the NO-π* orbital to the iron center. The limiting valence description of **A** is therefore a low spin d^6 Fe(II) center which strongly interacts with an essentially neutral $\bullet$NO radical. This conclusion has also been drawn by Olabe and co-workers[45,46] on the basis of similar DFT calculations for related complexes which are
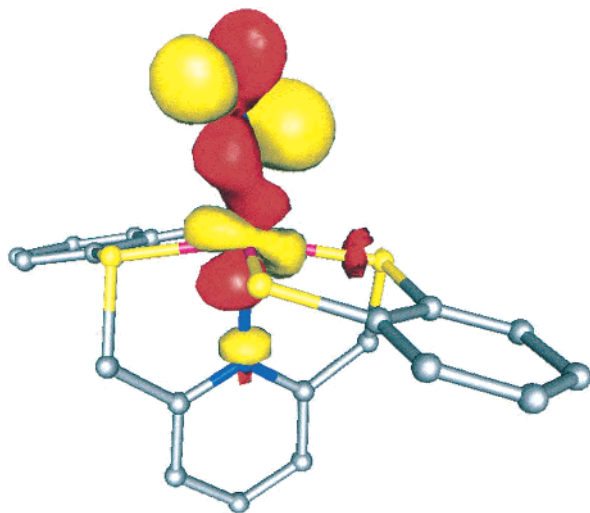
Figure 14. Singly occupied natural orbital of the complex [Fe(pyS₄)-(NO)] (**A**).

essentially in agreement with our results. However, it is stressed that the conclusion is not only supported by the calculations but also from the analysis of the available experimental data.

On the basis of the electronic structure description given previously, the available spectroscopic information can readily be interpreted. The large spin density on the NO ligand gives rise to a large ^{14}N-nitrogen hyperfine coupling seen experimentally and a small internal magnetic field established by the Mössbauer experiments. Because the SOMO is a σ orbital with respect to the Fe−NO bond, some spin density also arises at the axial position and is seen as a significant hyperfine splitting due to the pyridine nitrogen (Figure 14).

The results for the Mössbauer isomer shift are explained by two effects. First, the back-bonding ability of NO• is significantly smaller than that of NO⁺ because the π* orbitals of NO• are necessarily higher in energy than those of NO⁺ and interact, therefore, less strongly with the filled iron orbitals. In fact, the calculations predict a slightly higher back-bonding ability for NO• (~76% Fe character in the d_π orbitals, not shown) compared to CO (81% Fe character in the d_π orbitals, Figure 12). Consequently, one would expect a significantly larger isomer shift for **A** compared to **B** which is consistent with experiment. The second effect, however, is the transfer of electron density from the NO• ligand to the iron e_g based d_{z^2} orbitals. The two effects work in opposite directions because the π back-bonding will tend to decrease the electron density at the iron center while the charge donation will increase it. The net effect is that **A** has both, experimentally and theoretically, a ~0.13 mm/s larger isomer shift than the CO complex **E**. This indicates that the subtle

interplay of the two effects is well balanced in the calculations.

Conclusions

The most salient observation of the present study is the discovery of an $S = {}^1/_2 \rightleftharpoons S = {}^3/_2$ spin equilibrium for the octahedral (nitrosyl)iron complex **7** which is of the type {Fe−NO}^{7}.

By using a combination of experimental, spectroscopic techniques such as electron spin resonance and Mössbauer spectroscopy we have been able to describe the electronic structure of both forms in some detail.

Because of the observation that the Mössbauer parameters of all octahedral {Fe−NO}^{7} ($S = {}^3/_2$) species studied to date including **7** ($S = {}^3/_2$) are strikingly similar, we conclude, in accord with Solomon et al.'s proposal,[16,17] that all of these complexes contain a high spin ferric ion ($S = {}^5/_2$) which is intramolecularly strongly coupled to an NO⁻ ($S_{NO^-} = 1$) ligand.

In stark contrast, octahedral complexes of the type {Fe−NO}^{7} ($S = {}^1/_2$) are shown to contain a low spin ferrous ion (d⁶) and a coordinated •NO radical. Thus, the spin equilibrium of **7** encompasses two valence tautomers (redox isomers) rather than simple spin isomers.

Finally, we have shown that one electron oxidation of [Fe-(NO)(pyS₄)] ($S = {}^1/_2$) to the corresponding monocation [Fe-(NO)(pyS₄)]⁺ ({Fe−NO}^{7} → {Fe−NO}^{6}) is a ligand centered process where the coordinated •NO ligand is converted to a coordinated NO⁺. We have shown that an isomer shift difference of ~0.3 mm s⁻¹ on going from an {Fe−NO}^{7} to an {Fe−NO}^{6} species is readily accounted for by the varying π back-bonding ability of an •ṄO versus an NO⁺ ligand. We propose that all octahedral complexes of the {Fe−NO}^{6} type displaying small isomer shifts (~0 mm s⁻¹) and large quadrupole splitting parameters should be described as low spin ferrous species coordinated to an NO⁺ cation and *not* as iron(IV) ($S = 1$) containing an NO⁻ ($S = 1$) ligand.[6] This work also demonstrates that the prediction of spectroscopic and structural parameters by DFT methods is very powerful for the interpretation of experimental results. Thus, the combination of experiment and theory provides enhanced insight into the electronic structure and properties of non-heme (nitrosyl)−iron complexes.

Supporting Information Available: Magnetic Mössbauer spectra of **6** and **A** (Figure S1 and S2), X-ray crystallographic files, in CIF format, for compounds **1**, **4**, **5**, and **7**. This material is available free of charge via the Internet at http://pubs.acs.org.

IC011243A

(45) Gonzales, M. C.; Scherlis, D. A.; Estiu, G. L.; Olabe, J. A.; Estrin, D. A. *Inorg. Chem.* **2001**, *40*, 4127.
(46) Wanner, M.; Scheiring, T.; Kaim, W.; Slep, L. D.; Baraldo, L. M.; Olabe, J. A.; Zalis, S.; Baerends, E. J. *Inorg. Chem.* **2001**, *40*, 5704.